Paper

# Robust and Accurate Iris Segmentation Algorithm for Color and Noisy Eye Images

Przemysław Strzelczyk

*Research and Academic Computer Network NASK, Warsaw, Poland*

**Abstract—Efficient and robust segmentation of iris images captured in the uncontrolled environments is one of the challenges of non-cooperative iris recognition systems. We address this problem by proposing a novel iris segmentation algorithm, which is suitable both for monochrome and color eye images. The method presented use modified Hough transform to roughly localize the possible iris and pupil boundaries, approximating them by circles. A voting mechanisms is applied to select a candidate iris regions. The detailed iris boundary is approximated by the spline curve. Its shape is determined by minimizing introduced boundary energy function. The described algorithm was submitted to the NICE.I iris image segmentation contest, when it was ranked 11th and 10th out of total 97.**

***Keywords—biometrics, image segmentation, iris recognition.***

## 1. Introduction

One of the main problems with the iris recognition technology is a difficulty of acquiring good quality iris images in uncontrolled environments. In out-of-laboratory scenarios the probability of capturing undisturbed eye images not affected by noise, blurring and different kinds of occlusions is very low. Therefore the overall performance of iris-based biometric systems is highly influenced by the efficiency of segmentation algorithm. This paper introduces a new iris segmentation method that can be used to extract iris regions of both color and monochrome images. The simplified Hough transform for circle-like object is introduced which significantly reduces the computation time in the coarse localization of the pupil and the iris. The active contours based on splines are used to accurately estimate the iris boundaries and separate the iris from the eyelids and the eyelashes. A discrete optimization technique based on dynamical programming is used to robustly fit the active contours. The proposed method has been tested using color images from UBIRIS.v2 database from NICE.I (Noisy Iris Challenge Evaluation – Part I) competition [1], [2].

## 2. Related Work

The segmentation of the iris image in color and in the infrared light are slightly different. Iris recognition systems usually use monochrome images captured in infrared light, because for that light wavelengths the performance of the system is the highest. However color images contain more information which is usable for localization and segmentation. The NICE.I competition participants introduced segmentation algorithms which work on color images captured in visible light [3]–[10]. Tieniu Tan *et al.* in his winning algorithm use integrodifferential constellation method [3] which accelerates the integrodifferential operator used by Daugman [11], [12]. They also introduce the curvature model for eyelids detection and histogram based reflection removal. Luengo-Oroz, Faure and Angulo applied mathematical morphology for polar image filtering and approximated the iris boundary by looking for the shortest paths in generalized gray-level distances [4]. Labati and Scotti start with integrodifferential approach to coarsely localize the iris boundaries, then search for continuous boundary segments in polar image and interpolate the missing fragments using low-pass filtering [10]. They use the Gabor filters to detect and remove eyelashes. Dae Sik Jeong *et al.* detect pupil and iris simultaneously using two circular edge detectors [9]. If the number of specular reflection on the image is too low they use AdaBoost eye detection technique to check if it is possible that the eye is closed. Then they use adaptive convolution kernels to detect separable eyelashes and parabolic Hough transform to detect eyelids. Finally they apply color-bases iris area detection. Peihua Li *et al.* introduced limbic boundary localization algorithm combining Hough transform, K-means clustering and skin color modeling [8]. They detect eyelids using parabolic integro-differential operator combined with RANSAC-like techniques. Other autors usually use integrodifferential operator for iris and pupil localization, the parabolic Hough transform for eyelids removal and the local histogram thresholding for the eyelashes detection.

## 3. Color of an Eye

The light rays which travel through the pupil usually reflects many times before they come out of the eye interior. Most of the light is absorbed, so only a small amount of it is visible on the eye image making pupil a very dark object. However the fundus, which is the interior surface of the eye, and includes: retina, optic disc, macula, fovea and posterior pole, has a red tint for the human. Therefore under very high illumination, pupil may be observable as red, which we can experience in the red-eye effect. The human iris color ranges from brown to green, blue, gray and

hazel. It depends on many factors as texture, pigmentation, fibrous tissue and blood vessels. The melanin, which is the main iris pigment, is responsible for the colors which vary from yellowish-brown through dark brown to black depending on the concentration and the location of pigments. Other colors are observed due to selective reflection and absorption of biological molecules which are a part of different iris components (e.g., red color of hemoglobin in blood, colors produced by collagen in tissues, yellowish color of lipochrome). Some colors of iris may also be a result of the light diffraction and scattering (e.g., blue color is an effect of process called Tyndall scattering which has place in turbid layer of the iris). The sclera is the lightest part of the human eye. It contains mainly collagen and elastic fiber and it has usually white color, due to lack of pigment. A very light blue tint may be observable in children, for which the sclera is very thin, and a light yellow tint may be visible in elderly people due to fatty deposits or illness.

Due to the color richness of irises it is difficult to define their characteristic color subspace and distinguish the iris area based only on its color. However information about the color can be used to find the boundary between the iris and the sclera and between the iris and the pupil. If the reflections are removed the pupil area is the darkest part of the image regardless of the color component used. On the other hand, the iris area contains at least one color component which has a significant higher values than for the pupil area. Therefore in order to distinguish the pupil and the iris we generate a monochrome image with intensity values of each pixel equal to maximum intensity values of red (R), green (G) and blue (B) color components of the source eye image $I_{pupil\text{-}iris} = \max(I_R, I_G, I_B)$. The sclera is the lightest part of the eye image. Usually all the color components have very high intensity values in the sclera region. Therefore in offer to find the outer iris boundary we generate second monochrome image with intensity values equal to the minimum of the original image color components $I_{sclera\text{-}iris} = \min(I_R, I_G, I_B)$.

## 4. Segmentation algorithm

We noticed that the differences in intensity between the sclera and the iris are more significant that the differences between the iris and the pupil. Therefore our algorithm starts with the search for the outer iris boundary, and later searches its inner boundary. The pupil location and the size can be easily approximated when the iris size and the iris location is known.

In the first step of the segmentation we remove the highlights using histogram thresholding technique. Afterwards a directional image is computed, which for each image pixel approximate a local gradient of the intensity. Two filters based on directional derivarates of Gaussian are used to estimate the gradient components: horizontal $g_x(x,y)$ and vertical $g_y(x,y)$. The Gaussian-based filters are used in order to reduce the noise and high-frequency disturbances. The resulting array stores the gradient directions $\Theta(x,y) = \arctan(\frac{g_y(x,y)}{g_x(x,y)})$ and the gradient absolute values $\overline{g}(x,y) = \sqrt{g_x(x,y)^2 + g_y(x,y)^2}$. Afterwards a subset $S$ of all points is created, for which the absolute gradient magnitude is greater than a specific threshold. These points are candidate circle perimeter points. Similarly to the standard Hough transform an accumulator array $A(x,y,r)$ is prepared. Its values are initially set to zero. The algorithm updates the accumulator array for each candidate boundary point and for each radius with the absolute values of the gradient in the candidate boundary points as follows:

$$\begin{aligned} \widetilde{x}_i &\leftarrow x_i - r\cos\Theta(x_i,y_i), \\ \widetilde{y}_i &\leftarrow y_i - r\sin\Theta(x_i,y_i), \\ A(\widetilde{x}_i,\widetilde{y}_i,r) &\leftarrow A(\widetilde{x}_i,\widetilde{y}_i,r) + \alpha\overline{g}(x_i,y_i). \end{aligned}$$

The array value $A(x,y,r)$ is increased if and only if there is a probability that a candidate point from $S$ lay on the perimeter of the circle in the center in $(x,y)$ and radius $r$. To compensate the inaccuracy in the gradient magnitude and direction estimation, the accumulator array is convolved with 3-dimensional Gaussian filter. The local maxima in the smoothed accumulator array are the candidate circle centers. Next we use an iterated procedure to select $k$ local maxima which corresponds to the $k$ best candidates. In each iteration the global maximum is found by full search. The global maximum coordinates together with corresponding accumulator array value $A(x_j,y_j,r_j)$ are put on the centers candidate list. After that all the values of the array in the stored maximum neighborhood are set to zero to suppress any false center, and the algorithm proceed to the next iteration. When the process is finished a voting mechanism decide if the candidate passes to the next phase. The mechanism compares the accumulator array values of each two consecutive candidates. If the relative differences of the array values between the $i$th and ($i$+1)th maximum is greater that the predefined threshold, all the maxima from $i+1$ to $k$ are discarded. The range of the $x$, $y$ and $r$ parameters depends on the image size and the image capture conditions. Usually the circle center $(x,y)$ is within the image range but not too close to the image border. The iris radius is not greater than $1/3$ of the image height and the iris to pupil size ratio is usually between 1.5 and 3.

After the coarse approximation of iris and pupil center is finished the detailed boundary is modeled with splines. The spline is defined in the polar coordinates system anchored in the circle center. We use the 1st degree periodic spline based on the $K$ control points called later knots. The number of knots $K$ depends on the circle radius $R$ and spacing constant $c$ as follows: $K(r) = 2^{\lceil \log_2 \pi R \rceil - c}$. The spline is defined as a piecewise function, which returns the distance from the circle center based on the angle $\alpha$ and the parameters vectors $\widehat{\alpha}$ and $\widehat{r}$:

$$R(\alpha,\widehat{\alpha},\widehat{r}) = R^*(\alpha,\widehat{r}_k,\widehat{r}_{k+1},\widehat{\alpha}_k,\widehat{\alpha}_{k+1}) \text{ for } \alpha \in <\widehat{\alpha}_k,\widehat{\alpha}_{k+1}),$$

where

$$R^*(\alpha,\widehat{r}_k,\widehat{r}_{k+1},\widehat{\alpha}_k,\widehat{\alpha}_{k+1}) = \frac{1}{\Delta\alpha}\left(\widehat{r}_k(\widehat{\alpha}_{k+1}-\alpha) + \widehat{r}_{k+1}(\alpha-\widehat{\alpha}_k)\right)$$

$$\widehat{r}_0 \equiv \widehat{r}_K$$

The knots angular coordinates are fixed and uniformly distributed: $\widehat{\alpha}_k = k\Delta\alpha$, for $k = 0 \ldots K$, where $\Delta\alpha = \frac{2\pi}{K}$. The second coordinate of each knot $\widehat{r}_k$ is determined by the minimization of the introduced boundary energy function $E$. This energy function takes into account the intensity changes in the direction of radius calculated between the knots, the deviation of the resulting shape from the circle and the length of the boundary. The boundary is defined piecewise so the energy function $E$ can be decomposed into sum of partial energies $E_k$.

$$E(\widehat{\alpha},\widehat{r}) = \sum_{K}^{k=0} E_k(\widehat{\alpha},\widehat{r}),$$

where

$$E_k(\widehat{\alpha},\widehat{r}) = \lambda_1 \frac{\int_{\alpha_{k+1}}^{\alpha_k} -\frac{\partial(I^{\diamond} * G^{\diamond})}{\partial r}(R(\alpha,\widehat{\alpha},\widehat{r}),\alpha)\, d\alpha}{N(\widehat{\alpha},\widehat{r},k)} + \lambda_2 \left| R - \frac{1}{\Delta\alpha}\int_{\alpha_{k+1}}^{\alpha_k} R(\alpha,\widehat{\alpha},\widehat{r})\, d\alpha \right|.$$

The first term of the energy function calculates the blurred directional derivarate of the image intensity along the radius. The calculation is made for the polar image representation. The partial derivarate of the image $I^{\diamond}(r,\alpha)$ is convolved with the polar Gaussian filter $G^{\diamond}(r,\alpha)$. The resulting image emphasizes the iris or pupil boundary. The boundary points has higher intensity values in the resulting image and therefore the integral in the first term obtains lowest values for the curves which best fits the pupil and the iris boundaries. The normalizing function $N(\widehat{\alpha},\widehat{r},k)$ is used to compensate different path segment lengths. The second term of the equation introduces the weighted penalty for the deviation of the ring curve from the circle with radius $R$.

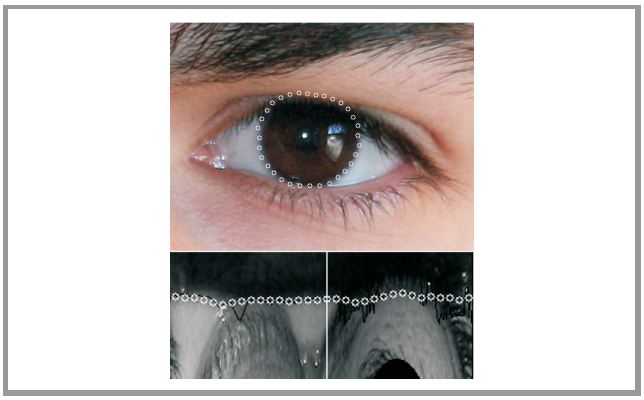

***Fig. 1.*** An eye image with the iris outer boundary approximated by the splines in the cartesian (top) and the polar (bottom) coordinate systems. Small circles indicate the spline knots positions. The white vertical line in the polar image shows the starting point of the spline shape optimization.

The knots second coordinates $r_k$ accept only discrete values, and should not change significantly between two neighboring knots. The differences from one knot to another should be small as the iris boundary is rather smooth. We could add the penalty for roughness to the energy function but we preferred to limit these differences as follows: $|r_k - r_{k+1}| \in \{0,1,\ldots,L-1,L\}$. In that way we obtained a discrete and limited space of the parameters to be optimized $r_k$. As the optimization of the energy function can be easily decomposed the dynamic programming can be used to find the optimal solution. The only problem is that the optimization horizon is periodic, and we need to fix one knot, or in other words we need to find the proper starting point. In our algorithm we used a simple heuristic for that purpose, which finds the stable boundary fragment and selects a point in the middle of it. Figure 1 shows the outer iris boundary approximated by the splines both in the original and the polar image. The small white circles indicate the knots positions.

Usually algorithm localizes more than one possible irise or pupil. To select the proper one we analyze the image intensity values near the shape boundary. A single score based on the t-test is used to select the best candidate. If we denote $X_o$ as the intensity values of the pixels near the boundary but outside the shape and $X_i$ as the intensity values of pixels near the boundary but inside the shape the score can be described as follows:

$$s = \frac{|\overline{X}_o - \overline{X}_i|}{\sqrt{0.5(\mathrm{Var}(X_o) + \mathrm{Var}(X_i))}}.$$

The two voting mechanisms, first based on accumulator array value and the second based on the $s$ successfully eliminate the non-iris and non-pupil image objects.

## 5. Tests and results

The presented algorithm was evaluated in *The Noisy Iris Challenge Evaluation, Part I*, organized by the Soft Computing and Image Analysis Group (SOCIA Lab) of the University of Beira Interior [1], [2]. The aim of the contest was to localize the undisturbed parts of the iris in the color iris images. The two parts of the second version of the UBIRIS database were used as a training set and an evaluation set . The UBIRIS.v2 consists of color eye images with the high level of noise to simulate the less controlled image acquisition conditions. The images include noise factors such as: poor focus, specular reflections, off-angle shots, no-iris images, rotation, motion blur, closed eyes, occlusions by eyelashes, eyelids, glasses and contact lenses. Some sample images from database are shown in Fig. 2

The database contain 500 close-up iris images and corresponding binary masks indicating the position of unoccluded iris area. The binary masks were prepared manually by the SOCIA Lab. The images were captured in visible light using digital camera from the distance of 3 to 7 m with resolution $400 \times 300$ pixels. A sample image with a binary mask from the training set is shown in Fig. 3.

The segmentation algorithms were evaluated using two performance indicators. The first one is the classification error

***Fig. 2.*** Sample images from UBIRIS.v2 database.

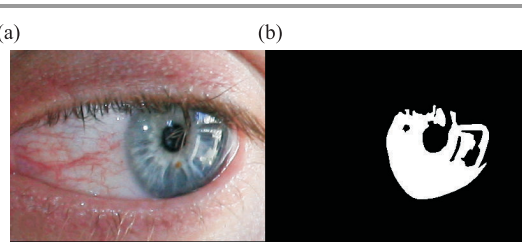


***Fig. 3.*** A sample image from UBIRIS.v2 database (a) with corresponding binary mask indicating iris area (b).

rate $E^*$, which is measured as the average proportion of the corresponding disagreeing pixels between the manually segmented images $M_i(x,y)$ and images segmented by the algorithm $A_i(x,y)$. It is calculated as the average normalized Hamming distance between the binary segmentation masks for all images as follows:

$$E^* = \frac{1}{N}\sum_i E_i^*,$$

$$E_i^* = \frac{1}{WH}\sum_{x,y}\left(M_i(x,y) \oplus A_i(x,y)\right),$$

where $H$ is the image height, $W$ is the image width and $\oplus$ is the binary ExOR operation.

The second performance indicator measures the average type-I and type-II error rates. It tends to compensate the disproportion between the a priori probabilities of the "iris" and "non-iris" pixels in the image. For a single image the second measure is defined as the average value of the the false-positives $FP_i$ and the false-negatives $FN_i$ as follows:

$$E^{\#} = \frac{1}{2N}\sum_i (FP_i + FN_i),$$

$$FP_i = 1 - \frac{\sum_{x,y}\left(M_i(x,y) \wedge A_i(x,y)\right)}{\sum_{x,y} M_i(x,y)},$$

$$FN_i = 1 - \frac{\sum_{x,y}\left(\neg M_i(x,y) \wedge \neg A_i(x,y)\right)}{\sum_{x,y} \neg M_i(x,y)},$$

where $\wedge$ is a binary AND operation (logical conjunction) and "$\neg$" is binary negation.

When the $E^*$ error rate was used our algorithm was ranked 11th out of 97 participants with score 3.41%. The best result obtained in the competition was 1.30% and the mean and the median of the first 10 best algorithms were 2.53% and 2.85% accordingly. When the $E^{\#}$ error rate was used our algorithm was ranked 10th with the score 11.70%. The lowest error rate in this classification was 5.50%, and the mean and the median of the first 10 algorithms were 8.28% and 7.30%. The scores of the first 24 participants are shown on Figs. 4 and 5. The algorithm was implemented

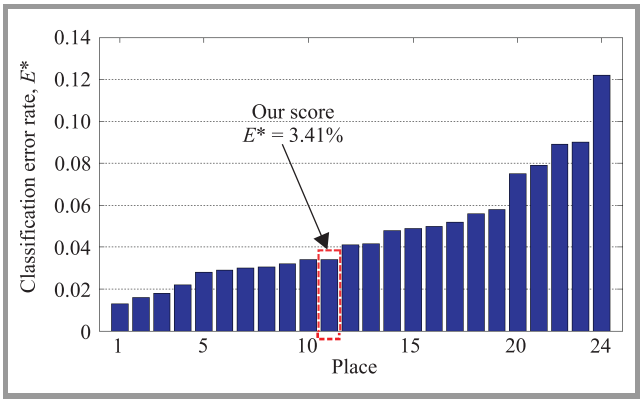


***Fig. 4.*** Classification error rates of the first 24 participants.

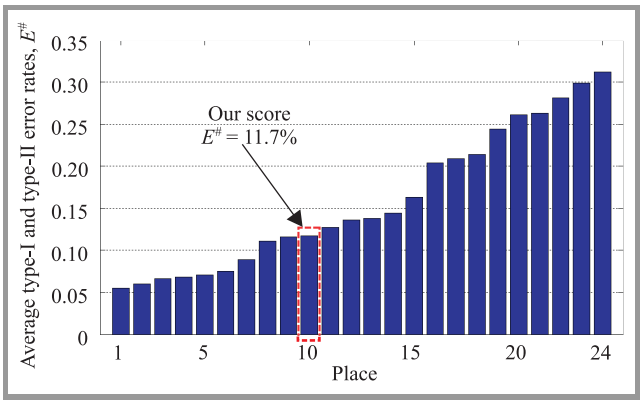


***Fig. 5.*** Average type-I and type-II error rates of the first 24 participants.

in C++ and it is worth to mention that although it was not optimized the segmentation time of the single eye image never exceeded 1 s for the images from UBIRIS database. In our opinion, the results were satisfactory and promising. The main advantages of the method were: the two-phase iris segmentation scheme with coarse localization based on Hough transform and fine segmentation based on spline based active contours. The voting system enabled proper selection of the genuine iris region and reflection removal in preprocessing reduced the errors in the coarse and detailed iris localization. Unfortunately the method has some drawbacks. The submitted version of the algorithm was not fully optimized for the search of pupil, and for some im-

ages the location, the shape and the size of the pupil was guessed based only on the training set and the iris outer boundary. The algorithm had also problems with images, where the iris was not visible. Moreover, it was found later the explicit eyelid, eyelashes and shadow detection models were very important in the NICE.I competition and all the leading algorithms had them implemented. Masking the areas occluded by eyelids and eyelashes significantly reduced the classification error. The conclusion of our tests is that the noisy iris image segmentation still remains an open problem, which deserves more efforts.

## 6. Conclusions

In this paper, we have presented an efficient and robust algorithm for the segmentation of the iris image captured in uncontrollable conditions and less-cooperative context. The algorithm was prepared in response to the NICE.I competition and works on color images, but after some modifications it can be applied to the state-of-art iris recognition devices. The performance evaluation results obtained in the competition shown that the presented approach is promising, but some improvements are required. There is a need to better model the eyelids and eyelashes areas and to introduce more context-based approach. The main advantage of the presented algorithm is the coarse-to-fine iris localization method which roughly approximates the iris shape with circle and later accurately tracks its boundaries with spline-based active contours.

## Acknowledgements

This paper has been financed by the Ministry of Science and Higher Education grant OR00 0026 07 "*A platform of secure biometrics implementations in personal verification and identification*".

## References

[1] H. Proença and L. A. Alexandre, "The NICE.I: noisy iris challenge evaluation, part I", in *Proc. Int. Conf. Biometr. Theory, Appl. Sys.*, Washington, USA, 2007, pp. 1–4.

[2] H. Proença and L. A. Alexandre, "UBIRIS: a noisy iris image database", *Lect. Notes Comput. Sci.*, vol. 3617, pp. 970–977, 2005 [Online]. Available: http://iris.di.ubi.pt

[3] T. Tan, Z. He, and Z. Sun, "Efficient and robust segmentation of noisy iris images for non-cooperative iris recognition", *Image Vision Comput.*, vol. 28, pp. 223–230, 2010.

[4] M. A. Luengo-Oroz, E. Faure, and J. Angulo, "Robust iris segmentation on uncalibrated noisy images using mathematical morphology", *Image Vision Comput.*, vol. 28, pp. 278–284, 2010.

[5] Y. Chen, M. Adjouadi, C. Han, J. Wang, A. Barreto, N. Rishe, and J. Andrian, "A highly accurate and computationally efficient approach for unconstrained iris segmentation", *Image and Vision Comput.*, vol. 28, pp. 261–269, 2010.

[6] W. Sankowski, K. Grabowski, M. Napieralska, M. Zubert, and Andrzej Napieralski, "Reliable algorithm for iris segmentation in eye image", *Image Vision Comput.*, vol. 28, pp. 231–237, 2010.

[7] P. de Almeida, "A knowledge-based approach to the iris segmentation problem", *Image Vision Comput.*, vol. 28, pp. 238–245, 2010.

[8] P. Li, X. Liu, L. Xiao, and Q. Song, "Robust and accurate iris segmentation in very noisy iris images", *Image Vision Comput.*, vol. 28, pp. 246–253, 2010.

[9] D. Sik Jeong, J. Won Hwang, B. Jun Kang, K. Ryoung Park, C. Sun Wonc, D.-K. Park, and J. Kim, "A new iris segmentation method for non-ideal iris images", *Image Vision Comput.*, vol. 28, pp. 254–260, 2010.

[10] R. D. Labati and F. Scotti, "Noisy iris segmentation with boundary regularization and reflections removal", *Image Vision Comput.*, vol. 28, pp. 270–277, 2010.

[11] J. Daugman, "New methods in iris recognition", *IEEE Trans. Sys. Man Cyb., Part B, Cybernetics*, vol. 37, no. 5, pp. 1167–1175, 2007.

[12] J. Daugman, "How iris recognition works?", *IEEE Trans. Circ. Sys. Video Technol.*, vol. 14, no. 1, pp. 21–30, 2004.

**Przemysław Strzelczyk** received his M.Sc. degree in Information Technology in 2005 from the Warsaw University of Technology, and he is currently a PhD candidate in the same field. Since 2005 he is with Reseach and Academic Computer Network (NASK) working for Biometric Laboratories, and within 2007 and 2009 he was research assistant at the Warsaw University of Technology. His main interests include: biometrics, security and methods of artificial intelligence.
e-mail: przemek.strzelczyk@nask.pl
Research and Academic Computer Network (NASK)
Wąwozowa st 18
02-796 Warsaw, Poland